Journal Homepage: www.ijrpr.com ISSN: 3049-0103 (Online)

International Journal of Advance Research Publication and Reviews

Vol 03, Issue 10, pp 709-715, October, 2026

NUMERICAL INVESTIGATION OF WS_2 AS A BUFFER LAYER IN CIGS SOLAR CELLS USING SCAPS-1D

Muhammad Khadijah Rabiu.[1] *, Babaji Garba.[2]

[1]Nigerian Building and Road Research Institute, Kano, Nigeria
[2,]Department of Physics, Bayero University, Kano, Nigeria
*khadijahrabiu47@outlook.com

ABSTRACT :

In this study, the performance of $CuInGaSe_2$ (CIGS) thin-film solar cells was evaluated using tungsten disulfide (WS_2) as an alternative to the conventional cadmium sulfide (CdS) buffer layer. Simulations were performed using SCAPS-1D under AM1.5G illumination and a temperature of 300 K. First, the CIGS solar cell with a CdS buffer was validated against a reference, yielding V_{oc} = 0.694 V, J_{sc} = 34.05 mA/cm^2, FF = 78.93%, and PCE = 18.66%. The CdS buffer layer was then replaced with a WS_2 buffer, and systematic optimization of its electron affinity, thickness, donor density, and interface defect density was carried out. The optimized WS_2 device achieved a PCE of 18.80%, V_{oc} = 0.694 V, J_{sc} = 34.2 mA/cm^2, and FF = 79.2%. WS_2 demonstrated greater interface defect tolerance, making it a strong candidate for an environmentally sustainable CIGS solar cell without toxic cadmium.

Keywords: Buffer, CdS, CIGS, Electron affinity, WS_2

1. Introduction

Copper Indium Gallium diSulphide (CIGS) solar cells occupy a prominent place thanks to their low production cost and excellent conversion efficiency, reaching 23.35% as published in 2019 (Nakamura et al., 2019). The CIGS solar cell has many merits, including a variable band gap (from 1.06 eV to 1.7 eV), and a high optical absorption coefficient. It also possesses radiation hardness, long-term stability, with a high absorption coefficient that allows the absorption of a major portion of the solar spectrum (Rasouli & Madani, 2020).

The most commonly used configuration of the CIGS solar cell is glass/Molybdenum/CIGS/buffer/i-Zinc Oxide/transparent conductive oxide (TCO), where cadmium sulfide (CdS) is widely used as the buffer layer due to its suitable bandgap (2.42 eV), high stability, and interface enhancement properties. However, the toxicity of Cadmium makes the use of CdS unfavorable from the viewpoint of human health and environmental protection (Rasouli & Madani, 2020). Thereby, its replacement by an environmental friendly material is one of the current challenges facing the scientific community.

Transition metal dichalcogenides (TMDCs) of the general formula MX_2 (M = transition metal; X = S, Se) have emerged as a promising class of buffer materials. Transition Metal Di-Chalcogenides (TMDCs) have great potential for use as flexible, ultra-thin photovoltaic materials in solar cells due to their favorable photon absorption and electronic transport properties (Roy, 2021).TMDCs exhibit high optical transparency, large carrier mobility, and tunable energy band structures. Light absorption coefficients can be achieved with TMDCs up to one order of magnitude higher than conventional direct-bandgap semiconductors (Aftab et al., 2023). Among the TMDC family, Tungsten disulfide (WS_2) has drawn the attention of the PV community due to its excellent properties such as tunable bandgap, high absorption coefficient (>10^5 cm^{-1}), good conductivity (10^{-3} Ω^{-1} cm^{-1}), high carrier mobility, non-toxicity, and earth-abundance for thin-film solar cell structures (Hassane et al., 2017; Sara et al., 2018).

In order to bring more insight into WS_2/CIGS solar cells, the Solar Cell Capacitance Simulator (SCAPS-1D) numerical tool has been used in this study. WS_2 as a CdS replacement in a standard CIGS device structure was investigated, evaluating the effects of electron affinity, buffer thickness, doping density, and interface defect density on the device performance. Temperature-dependent J–V analysis and quantum efficiency spectra are additionally provided to deepen the physical understanding of recombination mechanisms and spectral response of the solar cell.

2. Materials and Methods

In this work, the CIGS solar cell was modeled using the Solar Cell Capacitance Simulator (SCAPS-1D) version 3.3.10, developed at the University of Gent by Mark Burgelman. It has been widely employed to simulate the electrical characteristics, performance, and spectral response of several crystalline and thin film–based photovoltaic cells, including CIGS solar cells. One of the advantages of SCAPS is that its simulation results agree well with the corresponding experimental results. SCAPS employs Poisson's and the continuity equations for electrons and holes to estimate the steady-state band diagram, recombination profile, and carrier transport in one dimension (Moustafa et al., 2022). The Poisson's equation that connects the electrostatic potential to the charge, and the continuity equations for electrons and holes, are given by Equations 1, 2, and 3:

$$\frac{\partial}{\partial x}\left(\varepsilon_0 \varepsilon_r \frac{\partial \Psi}{\partial x}\right) = -q\left(p - n + N_D^+ - N_A^- + \frac{\rho}{q}\right) \quad (1)$$

$$-\left(\frac{1}{q}\right)\frac{\partial J_n}{\partial x} - U_n + G = \frac{\partial n}{\partial t} \quad (2)$$

$$-\left(\frac{1}{q}\right)\frac{\partial J_p}{\partial x} - U_p + G = \frac{\partial p}{\partial t} \quad (3)$$

Where Ψ is the electrostatic potential function, ρ is the charge density of defects, n and p are the free carrier concentrations N_A^- and N_D^+ are the densities of ionized acceptors and donors, ε_0 absolute permittivity, ε_r is the relative permittivity of the material, respectively. G is the generation rate, while J_p and J_n are the hole and electron current density.

2.1 CIGS cell structure

The $CuInGaSe_2$ model consists of n-ZnO/n-CdS/p-CIGS layers fabricated on a molybdenum-coated substrate. Molybdenum is used as the back contact layer because it has low contact resistance to the absorber layer and is also stable at the processing temperature (Biswas et al., 2023). The next layer is the $CuInGaSe_2$ absorber layer, an alloy of $CuInSe_2$ and $CuGaSe_2$ with a chalcopyrite structure. It is a p-type semiconductor material and the core layer of CIGS-based solar devices. The buffer layer forms a p-n junction with the absorber layer and protects the junction from chemical degradation and mechanical damage. It optimizes the band alignment of the cell and its electrical properties, making a wide depletion region with the p-type absorber layer (Ibrahem et al., 2013). As the window layer, ZnO is deposited on the buffer layer; it has an energy bandgap above 3.3 eV (Ehemba et al., 2015). The schematic diagram of the CIGS solar cell is shown in Fig. 1.

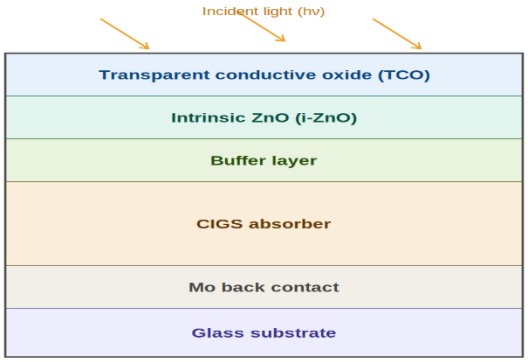


Fig. 1 - Schematic CIGS solar cell structure

2.2 Material parameters

To use the SCAPS software, some baseline parameters of the solar cell have to be defined as inputs. Table 1 shows the basic parameters used for this simulation (Biswas et al., 2023; Kafashan & Bahrami, 2024; Sobayel et al., 2021; Belhadji, 2022; Sobayel et al., 2020; Bin Rafiq et al., 2020; Oyedele & Aka, 2017; Khoshsirat et al., 2015; Ehemba et al., 2015). The absorption files used in the simulation were extracted from the SCAPS software. The study mainly focused on the optical and electrical properties of the buffer layer and its compatibility with CIGS; therefore, the interfacial recombination mechanism and the series and shunt resistance parameters were not considered. All simulations were performed under standardized illumination of the AM1.5 solar spectrum with an incident power density of 1000 W/m^2, and the operating temperature was set at 300 K.

Table 1 - Material parameters for all the layers

Parameter	CIGS	WS_2	i-ZnO	AZO
Thickness (μm)	2.2	0.06	0.08	0.350
Bandgap E_g (eV)	1.20	1.80	3.30	3.30
Electron affinity χ (eV)	4.50	4.40	4.60	4.60
Dielectric constant ε_r	13.6	13.6	9.0	9.0
N_c (cm^{-3})	2.2×10^{18}	2.2×10^{18}	2.2×10^{18}	2.2×10^{18}
N_v (cm^{-3})	1.8×10^{19}	1.8×10^{19}	1.8×10^{19}	1.8×10^{19}
μ_e ($cm^2\ V^{-1}\ s^{-1}$)	100	50	100	20
μ_h ($cm^2\ V^{-1}\ s^{-1}$)	25	10	25	10
N_D (cm^{-3})	0	1.0×10^{17}	1.0×10^{17}	1.0×10^{19}
N_A (cm^{-3})	2.0×10^{16}	0	0	0

Table 2 - Defect parameters for bulk layers and the CIGS/WS_2 interface

Parameter	CIGS	WS_2	CIGS/WS_2 interface
Defect type	Neutral	Neutral	Neutral
σ_e (cm^2)	1.0×10^{-13}	1.0×10^{-13}	1.0×10^{-15}
σ_h (cm^2)	1.0×10^{-13}	1.0×10^{-13}	1.0×10^{-15}
E_t (eV above E_v)	0.600	Mid-gap	0.600
N_t / N_{it} (cm^{-3} / cm^{-2})	1.0×10^{14}	1.0×10^{14}	1.0×10^{10}

To optimize the solar cell, the electron affinity of the absorber was kept constant at χ(CIGS) = 4.5 eV, while that of the buffer layer, χ(WS_2), was varied from 4.2 eV to 4.9 eV, which results in a variation of the conduction band offset from −0.3 eV to 0.4 eV. The conduction band offset (CBO) is the difference in electron affinity between the absorber (CIGS) and the buffer layer (WS_2). To find the optimal thickness and donor density of the WS_2 buffer layer, the thickness was varied from 0.1 μm to 0.2 μm, while the donor density was swept from 10^{15} cm^{-3} to 10^{19} cm^{-3} at the optimized buffer layer thickness; other parameters were kept constant.

The interface defect density at the CIGS/WS_2 junction was also increased from 10^{10} cm^{-3} to 10^{16} cm^{-2} at the optimized buffer layer electron affinity, thickness, and donor density. The J–V characteristics of the solar cell were simulated as a function of temperature from 280 K to 360 K for the WS_2 buffer layer device at its optimized parameters.

3. Results and Discussion

Table 3 - Simulation result compared with experimental data

Parameters	V_{oc} (V)	J_{sc} (mA/cm^2)	FF (%)	PCE (%)
CdS/CIGS (This work)	0.694	34.05	78.93	18.66
Experimental reference (Traoré et al., 2023)	0.7295	32.89	79.84	19.16

The CdS/CIGS solar cell was simulated and the obtained performance parameters were compared with experimental and simulation results corresponding to the standard CIGS cell with a CdS buffer layer. The simulated CdS/CIGS reference cell yielded a V_{oc} of 0.694 V, J_{sc} of 34.05 mA cm^{-2}, FF of 78.93%, and PCE of 18.66%. These results are in good agreement with previously reported numerical and experimental data in the literature.

3.1 Electron affinity optimization

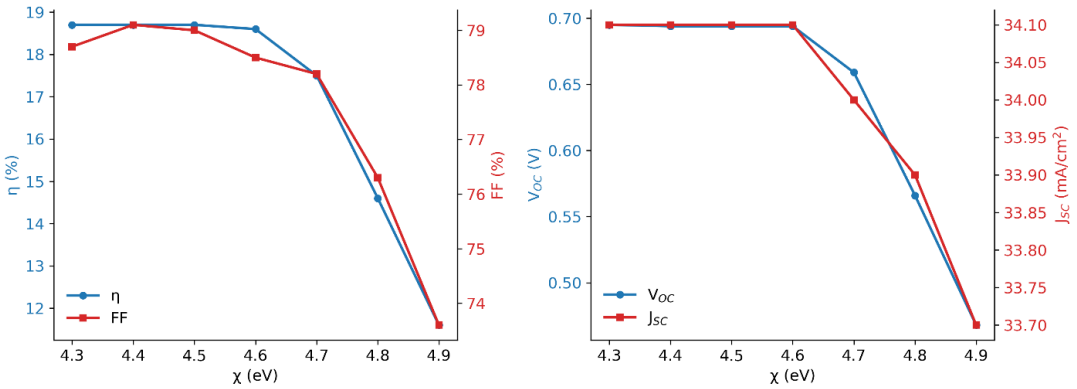


Fig. 2 - Dependence of the cell output parameters on the electron affinity of the WS_2 buffer layer

For WS_2, PCE was flat at 18.70% across χ = 4.30–4.50 eV (CBO = −0.20 to 0.00 eV), collapsing sharply beyond χ = 4.60 eV. The optimal χ = 4.40 eV (CBO = −0.10 eV) was adopted. The broader tolerance window of WS_2 (−0.20 to 0.00 eV) is a practical fabrication advantage, allowing less precise control of electron affinity during deposition.

3.2 Buffer thickness optimization

WS_2 achieved a maximum power conversion efficiency at a buffer layer thickness of 60–70 nm (PCE = 18.80%), and it declined beyond a thickness of 80 nm as a result of reduced J_{sc} due to parasitic optical absorption in the buffer. The V_{oc} and FF remained stable beyond 80 nm, while the J_{sc} dropped from 34.2 to 32.1 mA cm^{-2} between buffer thicknesses of 60 nm and 200 nm. An optimal buffer thickness of 60 nm was adopted for subsequent sweeps (Fig. 3).

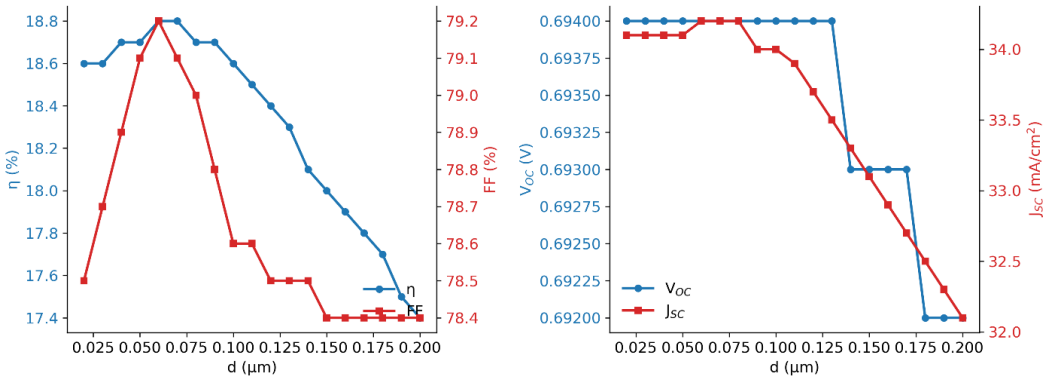


Fig. 3 - Dependence of the cell output parameters on buffer layer thickness

3.3 Donor doping density optimization

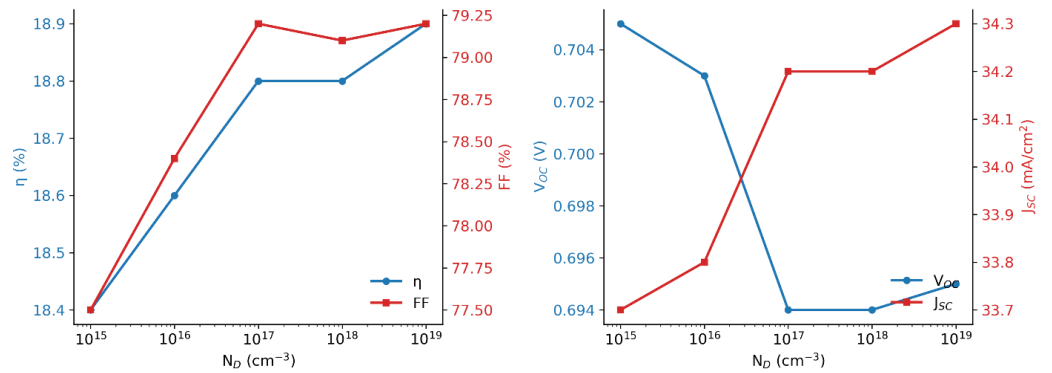


Fig. 4 - Output characteristics of the solar cell with changes in donor density

From Fig. 4, the maximum PCE of 18.80% is obtained at $N_D = 10^{17}$ cm^{-3}. The relatively high optimal donor density is directly attributable to the lower electron mobility of WS_2 (50 cm^2 V^{-1} s^{-1}), which requires higher doping to maintain adequate buffer conductivity and charge transport across the junction.

3.4 Interface defect density

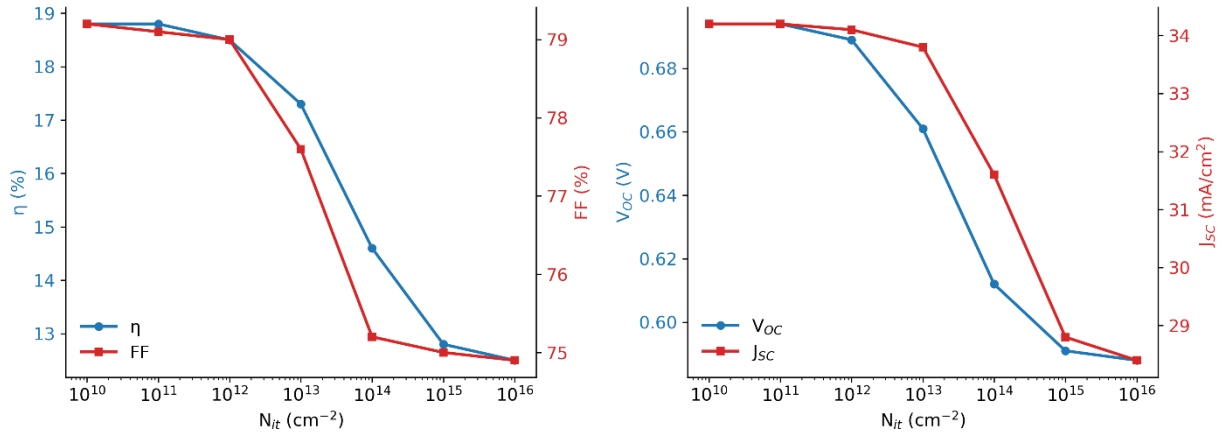


Fig. 5 - Output parameters of the cell as a function of interface defect density

The interface defect density N_{it} at the CIGS/WS_2 junction was swept from 10^{10} to 10^{16} cm^{-2} at the optimized χ, thickness, and N_D. WS_2 demonstrated substantially greater interface tolerance: PCE remained at 18.80% up to $N_{it} = 10^{11}$ cm^{-2}, declined gently to 18.50% at 10^{12}, and 17.30% at 10^{13} cm^{-2}, which is still competitive with the CdS baseline of 18.66%. Only beyond 10^{14} cm^{-2} did WS_2 performance degrade significantly.

The superior tolerance of WS_2 is attributed to its higher dielectric constant ($\varepsilon_r = 13.6$), which more effectively screens interface trap charges, and its higher optimal N_D, providing stronger band bending to partially compensate interface recombination. Given that experimentally deposited CIGS/buffer interfaces typically exhibit N_{it} in the range 10^{11}–10^{13} cm^{-2}, this finding makes WS_2 the more practically viable Cd-free buffer for real device fabrication.

3.5 Quantum efficiency

The quantum efficiency spectrum was calculated for the WS_2 buffer configuration over 300–1200 nm. In the short and mid-wavelength region (300–700 nm), the WS_2 device exhibits nearly identical QE to the CdS reference, rising from approximately 45% at 300 nm to a plateau of ≈95.3% between 380 and 700 nm. This confirms that WS_2 introduces no significant parasitic optical absorption at the optimized 60 nm thickness, as shown in Fig. 6.

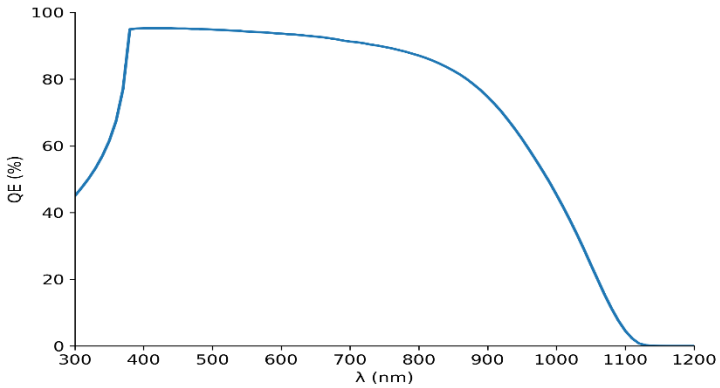


Fig. 6 - Quantum efficiency curve of the cell

Beyond 700 nm, the WS_2 QE curve shows the earliest roll-off among the three configurations, reflecting differences in the electric field distribution within the CIGS absorber arising from its band alignment. The device reaches zero QE at approximately 1033 nm, corresponding to the CIGS absorber bandgap of 1.20 eV. The J_{sc} calculated from QE integration was consistent with that from the J–V characteristic to within 1%, confirming current conservation.

3.6 Optimized cell

Table 5 presents the complete optimized photovoltaic parameters for the WS_2 buffer layer configuration benchmarked against the CdS reference (Fig. 7).

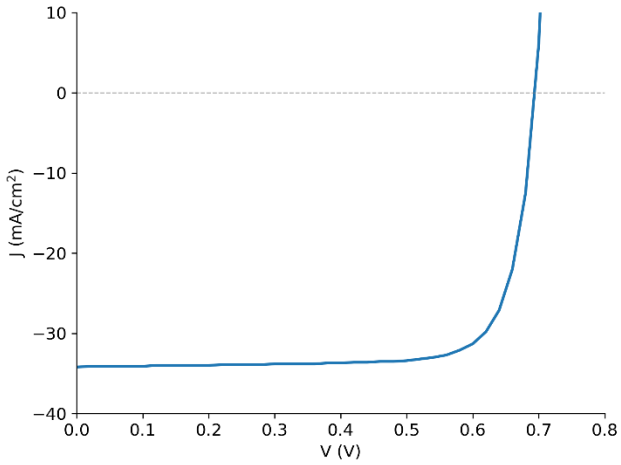


Fig. 7 - J–V curve of the optimized cell

4. Conclusion

This study has investigated the replacement of the CdS buffer layer in CIGS solar cells with WS_2 using SCAPS-1D. From the results obtained, it was shown that WS_2 is a viable cadmium-free alternative to CdS, achieving a PCE of 18.80% compared to 18.66% for the CdS baseline, without toxic cadmium. The optimal conduction band offset for WS_2 is −0.10 eV (shallow cliff) and the optimal buffer thickness is 60 nm, consistent with CIGS heterojunction physics. WS_2 requires higher doping (N_D = 10^{17} cm^{-3}) due to its lower electron mobility (50 cm^2 V^{-1} s^{-1}), directly linking intrinsic material transport properties to device optimization requirements. WS_2 exhibits substantially superior tolerance to interface defect density, maintaining competitive efficiency up to N_{it} = 10^{12}–10^{13} cm^{-2}, making it the more practically deployable Cd-free buffer layer for experimentally fabricated devices. Quantum efficiency spectra confirm no significant parasitic optical absorption in WS_2 at 60 nm thickness, with long-wavelength QE differences beyond 700 nm reflecting band alignment rather than optical losses.

References

- Belhadji, Y. (2022). Numerical Modeling of CuInxGa(1-x)Se2/WS2 Thin Solar Cell with an Enhanced PCE. *International Journal of Renewable Energy Development*, *11*(2), 393--401. https://doi.org/10.14710/ijred.2022.38527
- Bin Rafiq, M. K. S., Amin, N., Alharbi, H. F., Luqman, M., Ayob, A., Alharthi, Y. S., Alharthi, N. H., Bais, B., & Akhtaruzzaman, M. (2020). WS2: A New Window Layer Material for Solar Cell Application. *Scientific Reports*, *10*(1), 1--11. https://doi.org/10.1038/s41598-020-57596-5
- Biswas, S. K., Mim, M. K., & Ahmed, M. M. (2023). Design and Simulation of an Environment-Friendly ZrS2/CuInS2Thin Film Solar Cell Using SCAPS 1D Software. *Advances in Materials Science and Engineering*, *2023*. https://doi.org/10.1155/2023/8845555
- Ehemba, A. K., Dieng, M., Diallo, D., & Sambou, G. (2015). Influence of the donor doping density in CdS and Zn(O,S) buffer layers on the external quantum efficiency of Cu(In,Ga)Se2 thin film solar cell. *International Journal of Engineering Trends and Technology*, *28*(6), 280--286. https://doi.org/10.14445/22315381/ijett-v28p253
- Hassane, B., Abdennour, G., Benmoussa, D., & Abdelkader, B. (2017). Numerical simulation of CIGS solar cell with ZnS buffer layer. *Int. Conf. Automation, Control Engineering and Computer Science (ACECS) Proc. Eng. Technol.*, *21*, 1.
- Ibrahem, M. A., Lan, T. W., Huang, J. K., Chen, Y. Y., Wei, K. H., Li, L. J., & Chu, C. W. (2013). High quantity and quality few-layers transition metal disulfide nanosheets from wet-milling exfoliation. *RSC Advances*, *3*(32), 13193--13202. https://doi.org/10.1039/c3ra41744a
- Kafashan, H., & Bahrami, A. (2024). CIGS solar cells using ZrS2 as buffer layer: Numerical simulation. *Optik*, *298*, 171594. https://doi.org/https://doi.org/10.1016/j.ijleo.2023.171594
- Khoshsirat, N., Md Yunus, N. A., Hamidon, M. N., Shafie, S., & Amin, N. (2015). Analysis of absorber layer properties effect on CIGS solar cell performance using SCAPS. *Optik*, *126*(7--8), 681--686. https://doi.org/10.1016/j.ijleo.2015.02.037
- Moustafa, M., Al Zoubi, T., & Yasin, S. (2022). Optoelectronics Simulation of CIGS-Based Solar Cells Using a Cd-Free Nontoxic ZrSxSe2−x as a Novel Buffer Layer. *Brazilian Journal of Physics*, *52*(4), 1--10. https://doi.org/10.1007/s13538-022-01146-z
- Nakamura, M., Yamaguchi, K., Kimoto, Y., Yasaki, Y., Kato, T., & Sugimoto, H. (2019). *Cd-Free Cu (In , Ga)(Se , S) 2 Thin-Film Solar Cell With Record Efficiency of 23 . 35 %*. 1--5. https://doi.org/10.1109/JPHOTOV.2019.2937218
- Oyedele, S. O., & Aka, B. (2017). Numerical Simulation of Varied Buffer Layer of Solar Cells Based on Cigs. *Modeling and Numerical Simulation of Material Science*, *07*(03), 33--45. https://doi.org/10.4236/mnsms.2017.73003

- Rasouli, F., & Madani, M. R. (2020). Analysis of CIGS-based thin film tandem solar cell with ZnS buffer layers. *Optical and Quantum Electronics*, *52*(11), 1--10. https://doi.org/10.1007/s11082-020-02590-4
- Sara, B., Baya, Z., & Zineb, B. (2018). Investigation of Cu(In, Ga)Se2 solar cell performance with non-cadmium buffer layer using TCAD-SILVACO. *Materials Science- Poland*, *36*(3), 514--519. https://doi.org/10.2478/msp-2018-0054
- Sobayel, K., Rahman, K. S., Karim, M. R., Aijaz, M. O., Dar, M. A., Shar, M. A., Misran, H., & Amin, N. (2018). Numerical modeling on prospective buffer layers for tungsten di-sulfide (WS2) solar cells by scaps-1D. *Chalcogenide Letters*, *15*(6), 307--315.
- Sobayel, K., Shahinuzzaman, M., Amin, N., Karim, M. R., Dar, M. A., Gul, R., Alghoul, M. A., Sopian, K., Hasan, A. K. M., & Akhtaruzzaman, M. (2020). Efficiency enhancement of CIGS solar cell by WS2 as window layer through numerical modelling tool. *Solar Energy*, *207*(July), 479--485. https://doi.org/10.1016/j.solener.2020.07.007
- Sobayel, M. K., Chowdhury, M. S., Hossain, T., Alkhammash, H. I., Islam, S., Shahiduzzaman, M., Akhtaruzzaman, M., Techato, K., & Rashid, M. J. (2021). Efficiency enhancement of CIGS solar cell by cubic silicon carbide as prospective buffer layer. *Solar Energy*, *224*, 271--278. https://doi.org/10.1016/j.solener.2021.05.093
- Traoré, B., Ouédraogo, S., Oubda, D., Bawindsom Kébré, M., Zongo, A., Sankara, I., & Zougmoré, F. (2023). Enhancing Strategy CIGS Solar Cell Performance Through a New ZnSe Buffer Layer. *Physics and Materials Chemistry*, *9*(1), 1--7. https://doi.org/10.12691/pmc-9-1-1